acta physica slovaca vol. 45 No. 6, 617 – 624 December 1995

# INTERPLAY OF SURFACE EFFECTS AND GRADUAL ABSORPTION IN MULTISTEP REACTION CALCULATIONS[1]

**M. Avrigeanu[2], A. Harangozo, V. Avrigeanu**
*Inst. of Physics and Nucl. Engn., P.O.B. MG-6, 76900 Bucharest, Romania*

**A.N. Antonov**
*Institute of Nuclear Research and Nuclear Energy, Sofia 1784, Bulgaria*

Received 23 October 1995, accepted 27 October 1995

Modified particle–hole state densities by using energy–dependent s.p.s. densities of excited particles and holes, corrected for the finite potential well, and Pauli, pairing and shell effects, have been incorporated into the FKK formalism. Effects of the preequilibrium emission in the region of nuclear surface have been taken into account by adoption of average Fermi energies calculated in the local density approximation, for the first step of the MSD/MSC processes.

## 1. Introduction

The preequilibrium (PE) reactions are described within both the semiclassical models and quantum–statistical theories as passing through a series of particle–hole excitations caused by two–body interactions. If the initial target–projectile interaction is within the diffuse nuclear surface then the energy of the possible hole excitation due to the shallower nuclear potential in this region will be limited [1]. On the other hand, the account for the density dependence of the effective $N$–$N$ interaction strength $V_0$, which is treated as the only free parameter of the quantum-statistical Feshbach–Kerman–Koonin (FKK) theory [2], has provided a consistent description [3] of the multistep direct (MSD) and multistep compound (MSC) processes.

Actually, an average Fermi energy derived from a nuclear density which is averaged along the projectile path (also as a function of the angular momentum $l$) have been used in the Geometry Dependent Hybrid model [4]. The Fermi energy averaged over the whole nuclear radius (i.e. for $l$=0) of ~30 MeV was obtained, then it decreases for higher partial waves. On the other hand, Kalbach [1] described the surface effects in a broad range of mass and energy by using an empirical mean effective Fermi energy with values between 11 and 25 MeV in the region of the first interaction. The reaction–model

[1] Presented at the International Symposium on Pre-Equilibrium Reactions, Smolenice Castle, 23 – 27 October, 1995

[2] email: MAVRIG@ROIFA.BITNET

0323-0465/95 

independent role of the surface effects in particle–hole state densities is also proved by the recent FKK calculations of $(n,n')$ and $(n,p)$ reactions at 7 to 26 MeV on $^{46,48}$Ti, $^{56}$Fe, and $^{93}$Nb [5].

Various quantities which can give evidences for a possible surface localization of the PE reactions at low energies are considered within this work. Next, the surface effects which are due to the shallower nuclear potential are taken into account within FKK formalism. Finally, these effects are compared with the ones due to recent consideration in FKK theory of gradual absorption from the entrance channel [6].

## 2. Average Fermi energy in the first *PE* two–body collision

The probability of the first interaction between the projectile and a nucleon of the target nucleus to occur in the diffuse nuclear surface can be expressed as a function of the mean free path (m.f.p.) $\lambda$ of the incident particle in nuclear matter (e.g. [7]). Since it has been shown [8, 9] that only a local m.f.p. $\lambda(r)$ should be considered for finite nuclei, alternative quantities like the absorption probability are considered to be more meaningful. First, for nucleons under the action of a local energy–dependent complex optical model potential (OMP) $U+iW$, the local m.f.p. is

$$\lambda(r) = -\frac{\hbar}{W(r)} \cdot \left[\frac{E-U(r)}{2m}\right]^{1/2} \qquad (1)$$

where $m$ is the nucleon mass. The energy- and radial–dependences of the phenomenological imaginary OMP (e.g. [10]) are responsible for the corresponding dependences of the local m.f.p. shown in Fig. 1 for neutrons incident on the target nucleus $^{93}$Nb at typical low energies involved in PE studies [11]. The depths of the OMP imaginary parts are small at the lowest energies (due to the Pauli–blocking effect) and they increase with the energy. This results in the m.f.p. higher values in the nuclear interior for small energies and its lower values at higher energies. On the other hand, the surface peaking of the imaginary potential at low energies causes a minimum of $\lambda(r)$ in the region of the nuclear surface, as deeper as lower the energy. The OMP transition from surface to volume character for incident energies increasing to medium values, leads to a radial dependence of $\lambda$ which gives the usual constant values in the central region of the nucleus. As can be expected, the m.f.p. is increasing quickly when the nuclear density and consequently the potential well are vanishing.

Next, a particle with constant m.f.p. within an uniform–density nuclear matter has the probability for the first interaction with a nucleon in the radial interval $\Delta$ at a distance $r$, equal to $e^{-r/\lambda}(1-e^{-\Delta/\lambda})$ (e.g. Eq. (A3) of Ref. [12]). The assumption of a sharp cut–off approximation for both the nucleus density and $\lambda$, with finite value of the latter up to a radius $R$ at which the incident particle is *entering* the nucleus, would lead to the similar form $e^{-R/\lambda}e^{r/\lambda}(1-e^{-\Delta/\lambda})$. The final consideration of the radial–dependence $\lambda(r)$ provides the probability for a first collision in the interval $\Delta$ at the nuclear radius $r$ [11]

$$P(r,\Delta) = \left[\exp\left(-\int_r^{R_s}\frac{dr'}{\lambda(r')}\right)\right]\cdot\left[1-\exp\left(-\int_{r-\Delta}^{r}\frac{dr'}{\lambda(r')}\right)\right] \qquad (2)$$



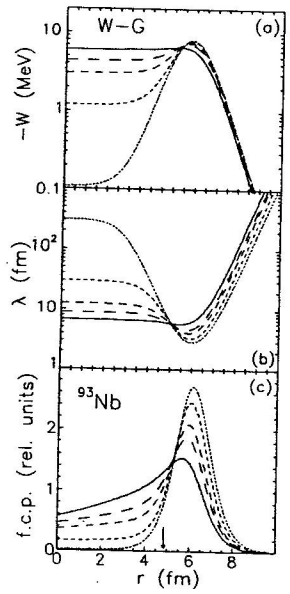


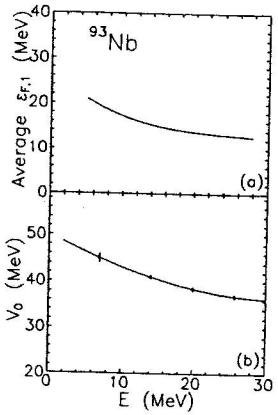


Fig. 2. Calculated average Fermi energy for the first two–body collision (a), and effective interaction strength $V_0$-values obtained by FKK analysis (b) for neutron–induced reactions on $^{93}$Nb, as function of the incident energy.

Fig. 1. Radial dependence of the (a) imaginary optical potential [10], (b) corresponding local m.f.p., and (c) first two–body collision probability for incident neutrons on $^{93}$Nb at incident energies of 7 (dotted), 14 (short–dashed), 26 (dashed), 35 (long–dashed), and 50 MeV (full curves).

The quantity in the first set of square brackets represents the probability of the incident particle to penetrate the target nucleus without any interaction up to a point of radius $r$, while the second one gives the probability that the first collision with a target nucleon happens in the next $\Delta$-radial step of the particle trajectory. The starting point of this path has been taken at the radius $R_s = r_0 A^{1/3} + 6a$ at which the surface imaginary potential of reduced radius $r_0$ and diffuseness $a$ is one percent of its central depth. The probability (2) has been calculated numerically by using the $\lambda(r)$-values given by Eq. (1), for a $\Delta$-value of 0.01 fm. Actually, values of $\Delta$ lower than e.g. 0.1 fm give similar maxima and relative shapes of this probability at different incident energies. The results obtained for incident neutrons on $^{93}$Nb are shown in Fig. 1(c).

The surface character of the first two–body interaction is proved by the maximum of the first–collision probability (f.c.p.), higher at the lower incident energies, which is mainly due to the probability for the collision to occur in the $\Delta$-interval at radius $r$. The latter has maxima at slightly lower radii with the increase of the energy and becomes indeed rather constant in the nuclear interior at higher energy. The still existing decrease of the f.c.p. to the centre of nucleus in this limit is given by a constantly–decreasing probability of the incident particle to penetrate the target nucleus without any interac-

tion up to the radius $r$. Further consideration of the angular momentum could provide better accuracy of the results and give an additional information for processes at higher incident energies.

The calculated probabilities for the first PE two–body collision (*first step*) can be used now to obtain average quantities at the nuclear surface, as it is the potential well depth reduced in this case to an empirical effective value in Ref. [1]. The local Fermi energies [7, 12, 13, 14] determined by the realistic nuclear density $\rho(r)$ [15] as

$$\varepsilon_{\rm F}(\rho(r)) = \frac{\hbar^2}{2m}\left(\frac{3\pi^2}{2}\rho(r)\right)^{2/3} \tag{3}$$

can be used to calculate the first–step average Fermi energy in the local density approximation (LDA)[11]

$$\overline{\varepsilon}_{\rm F1} = \frac{\int_{R'-\lambda}^{R_s}\varepsilon_{\rm F}(\rho(r))\rho(r)r^2{\rm d}r}{\int_{R'-\lambda}^{R_s}\rho(r)r^2{\rm d}r} \tag{4}$$

along the radial trajectory of the incident nucleon in the region of the first two–body collision. This region was considered from the radius $R_s$ at which the nuclear density is lower than one percent of its central value, similarly to the limit used for the f.c.p. calculation but with reference to the Woods–Saxon form factor of the density [15]. On the other hand, the f.c.p.–maximum radius $R'$ less the reduced wavelength $\lambda$ of the incident particle, has been considered as the inner end of the path related to the first collision with a nucleon of the target nucleus. The introduction of $\lambda$ takes into account the uncertainty in the position of the projectile. Its smaller values at higher energies lead to a reduced account of the low–radius side of the f.c.p. peak. Therefore, in order to apply this analysis also for energies larger than 30 MeV, this inner limit should be decreased. However, the inclusion of the angular momentum which enhances obviously the surface localization, could yet avoid this correction. The $\overline{\varepsilon}_{\rm F1}$-values for incident neutrons on the target nucleus $^{93}$Nb are shown in Fig. 2(a).

## 3. Surface effects in multistep reaction analyses

An improved particle–hole state density including different energy–dependences of the excited–particle and hole state densities has recently been used [16] in the GDH semiclassical model [4], and for the MSD and MSC processes in the framework of the FKK theory as described elsewhere [5].

Following Kalbach [1] we have considered the PE surface effects by limiting the possible excitation energy of the hole degree of freedom. In this respect the Fermi energy of ~38 MeV, which corresponds to the central depth of the potential well, was replaced initially [5] with an average effective Fermi energy for the *first* two–body projectile–target interaction. In order to get a first sight on the proper size of surface Fermi energy, this effective quantity was the only free parameter in the respective FKK calculations while the strength $V_0$ was kept in the range found in previous analyses performed with nearly the same parameters. Then, the fitted effective Fermi energies obtained in that



FKK analysis have been found very close to the LDA average Fermi energies [11]. It has been thus proved that use of surface average Fermi energies is meaningful.

Furthermore, we are using in this work the LDA average Fermi energies in the FKK first step calculations, while the strength $V_0$ has been again considered as the only adjustable parameter of the MSD model. The Milano computer code MUDIR [17] has been involved, enlarged by inclusion of the modified particle–hole state densities and the spherical optical model code SCAT2 [18].

The collective enhancement of the direct scattering cross section due to low–energy surface vibrations of quadrupole and octupole multipolarity, which is not described by the FKK model, has been included by means of the DWBA method. The DWUCK4 code [19] and a conventional collective form–factor have been thus used, and deformation parameters $\beta_L$ were derived from results of similar macroscopic DWBA analyses by imposing the condition of equal deformation lengths $\delta_L = R\beta_L$ (where R is the radius of the respective optical potentials).

Following Marcinkowski *et al.* [6], we have used for MSC emission from particle–hole bound states ($Q$ space) the modified FKK theory for gradual absorption of the reaction flux through $P \rightarrow Q$ transitions at the subsequent stages $M$ of the reaction. The MSC cross sections have been calculated by means of an enlarged version of the code GAMME [20] including the optical model code SCAT2 (see also [21]) and the present exciton–state density [5]. Finally, the code STAPRE–H95 [16, 22, 23] is used for the $r$–stage and second–chance emission calculations.

## 4. Results and discussion

The double–differential cross-section analysis at intermediate emission energies has been used in order to determine the strength $V_0$. Actually, at the incident energy of 7 MeV the MSD contribution is at most one order of magnitude smaller, while it accounts for nearly all emission cross section at incident energies of 20 and 25.7 MeV (Fig. 3). Therefore, the fit of the $(n,n')$ angular distributions (Fig. 3) provides $V_0$-values of 45±1, 41±0.5, 38.5±0.5, and 37±0.5 MeV for the incident energies from 7 to 25.7 MeV, while the analysis of the $(n,p)$ data at 14.1 MeV (Fig. 4) yields $V_0$=35±0.5 MeV. Since the FKK theory does not include the collective vibrational effects, which are significant even at the intermediate emission energies [24], the neutron–emission data at forward angles are systematically underestimated. Moreover, the data for $^{93}$Nb at the incident energy of 7 MeV and higher emission energies include already the collective excitation of the low–lying states; it seems that additional states or higher deformation parameters could provide the experimental forward–peaking.

The change at various incident energies of the MSD and MSC calculated cross sections has been checked by analyzing the angle–integrated spectra for neutron emission at the four incident energies (Fig. 5). There is an overall good agreement between the FKK results and experimental data, which is concludent mainly for the MSD component. The MSC processes have already no contribution above the emission energy of 10 MeV, at the incident energies of 20 and 25.7 MeV, so that the intermediate–energy region of respective spectra is given fully by the MSD cross section. Actually, the exper-

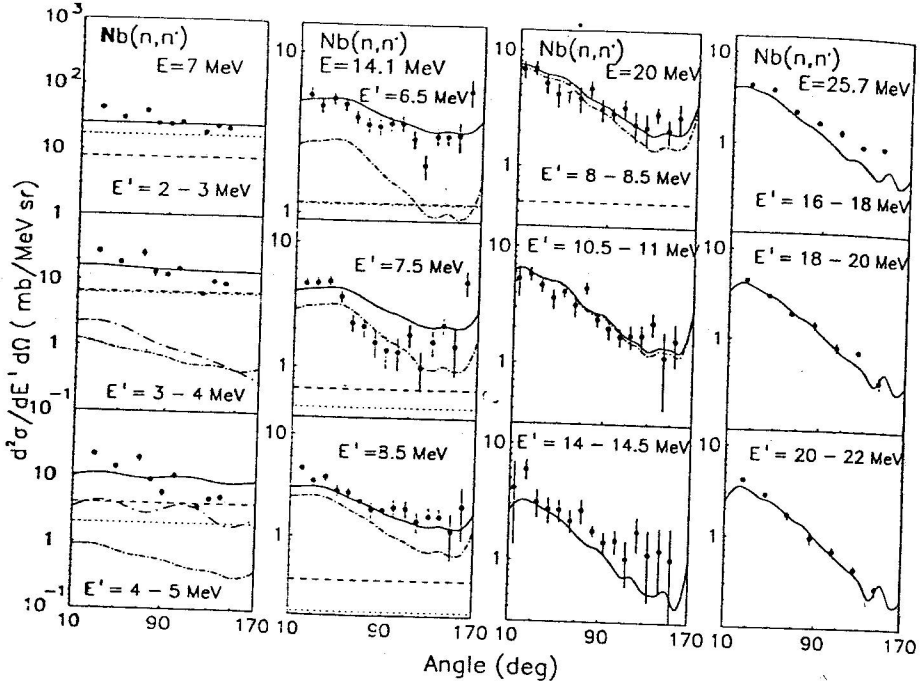


Fig. 3. Comparison of FKK and experimental angular distributions of neutrons from 7, 14.1, 20, and 25.7 MeV neutron–induced reactions on $^{93}$Nb. Total cross sections (solid curves) include contributions of direct collective excitation (long dashed–dotted), MSD (dotted–dashed), MSC (dashed) and statistical $r$–stage (dotted) processes. For experimental data see [5].

imental spectra at the incident energy of 25.7 MeV were given just above the sequential decay and MSC region.

The effect of replacing a constant s.p.s. density $g = 6a/\pi^2$ by energy–dependent quantities $g_p$ and $g_h$, and next by using the surface average Fermi energies, is discussed for the calculated emission spectra from 14 MeV $(n,n')$ and $(n,p)$ reactions on $^{93}$Nb. In each case the fit of the respective experimental angular distributions provides the $V_0$-values shown in Fig. 6. The allowance for surface effects in FKK calculations works in one sense similarly to the consideration of the gradual absorption by $P \rightarrow Q$ transitions at subsequent reaction stages: the MSC cross sections in the first stages are reduced in magnitude, in favour of the $r$–stage equilibrium emission. This has been shown especially when the same surface–effects analysis is carried out without gradual absorption [5]. The MSC proton–emission contribution was stronger in this case, so that the surface effects has decreased it nearby the experimental spectrum. It can be seen now that the two classes of effects are not disjunctive, and their sum leads to better description of data.

If the same calculations are done without gradual absortion by $P \rightarrow Q$ transitions at subsequent stages, the MSC component is over MSD unless the highest few MeV of



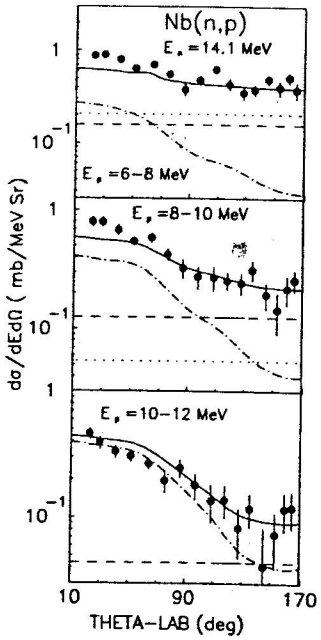


Fig. 4. The same as in Fig. 3, for proton emission at the incident energy of 14.1 MeV on $^{93}$Nb.

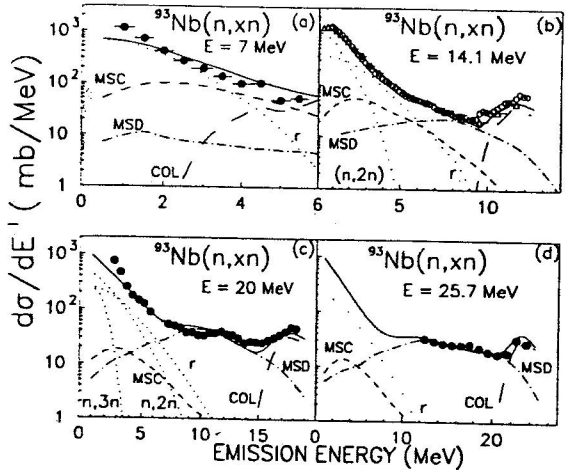


Fig. 5. Comparison of calculated (FKK) and experimental angle–integrated spectra for $^{93}$Nb$(n,n')$ at (a) 7 (b) 14.1, (c) 20, and (d) 25.7 MeV. The curve meaning is the same as in Fig. 3, with addition of the main sequential–decay cross sections (dotted curves).

spectra. The final results obtained by taking into account both the surface effects and gradual absorption are in agreement with Marcinkowski *et al.* [6, 25] the MSC emission of both neutrons and protons being decreased in the benefit of the HF statistical emission staying for equilibrium $r$–stage.

**Acknowledgments** The authors would like to thank Peter E. Hodgson who suggested this investigation and for useful discussions. This work was carried out under the Romanian Ministry of Research and Technology Contract No. 150B-A3 and the Bulgarian National Science Foundation Contract No. Phi–406.

## References

[1] C. Kalbach: *Phys. Rev. C* **32** (1985) 1157
[2] H. Feshbach, A. Kerman, S. Koonin: *Ann. Phys. (NY)* **125** (1980) 429
[3] R. Bonetti, L. Colombo: *Phys. Rev. C* **28** (1983) 980
[4] M. Blann: *Nucl. Phys.* **A213** (1979) 570 ;
M. Blann, H.K. Vonach: *Phys. Rev. C* **28** (1983) 1475
[5] M. Avrigeanu *et al.*: *in Proc. of the 7th Int. Conf. Nucl. Reaction Mech., Varenna 1994 (Ed. E. Gadioli).* Ric. Sci. Educ. Perm., Milano 1994, p. 165;
M. Avrigeanu *et al.*: Report NP-85-1995, IPNE Bucharest 1995
[6] A. Marcinkowski *et al.*: *Nucl. Phys. A* **561** (1993) 387

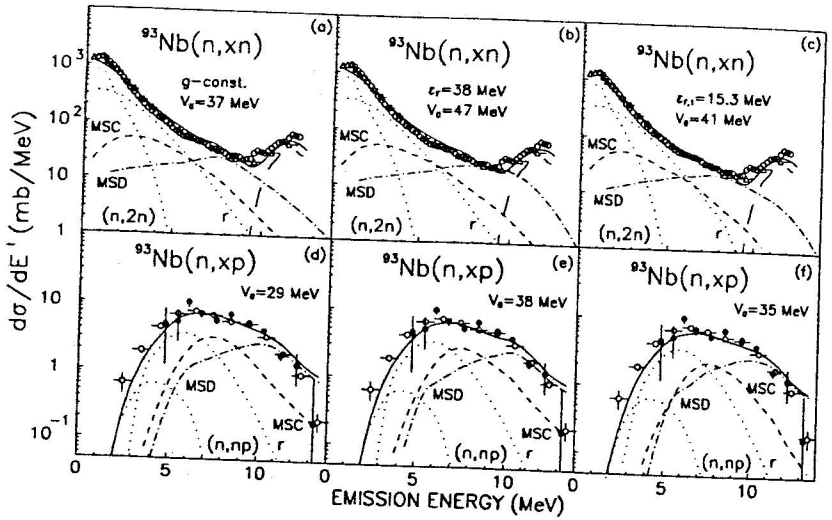


Fig. 6. Comparison of calculated (FKK) and experimental angle–integrated spectra for $(n, n')$ and $(n, p)$ reactions at 14.1 MeV on $^{93}$Nb. The calculated curves, with the same meaning as in Fig. 5, are obtained by using: (a,d) constant s.p.s. density $g = 6a/\pi^2$, (b,e) energy–dependent $g_p$ and $g_h$ with the Fermi energy of 38 MeV, and (c,f) the average Fermi energy 15.3 MeV in the $N$=1 MSD and MSC reaction stages. For experimental data see Ref. [5].

[7] K. Kikuchi, M. Kawai:*Nuclear Matter and Nuclear Reactions.* North-Holland, Amsterdam 1968

[8] R.M. DeVries, N.J. DiGiacomo: *J. Phys. G* **7** (1981) L51

[9] R.W. Hasse, P. Schuck: *Nucl. Phys. A* **445** (1985) 205

[10] R.L. Walter, P.P. Guss: *Rad. Effects* **95** (1986) 73

[11] M. Avrigeanu, A.N. Antonov, A. Harangozo, V. Avrigeanu: *to be published*

[12] K. Chen *et al.*: *Phys. Rev.* **166** (1968) 949

[13] G.W. Greenlees *et al.*: *Phys. Rev.* **171** (1968) 1115

[14] A.N. Antonov, P.E. Hodgson, I.Zh. Petkov: *Nucleon Momentum and Density Distribution in Nuclei.* Clarendon Press, Oxford 1988

[15] J.W. Negele: *Phys. Rev. C* **1** (1970) 1260

[16] M. Avrigeanu, V. Avrigeanu: *J. Phys. G* **20** (1994) 613

[17] R. Bonetti, C. Chiesa: *MSD code system.* Universita di Milano *(unpublished)*

[18] O. Bersillon: Note CEA-N-2227. CEN-Bruyeres-le-Chatel, 1981

[19] P.D. Kunz: *DWUCK4 user manual.* OECD/NEA Data Bank 1984

[20] R. Bonetti, M.B. Chadwick: Report OUNP-91-16, Oxford University, 1991

[21] M. Avrigeanu, P.E. Hodgson, A.J. Koning: *J. Phys. G* **19** (1993) 745

[23] M. Uhl, B. Strohmaier: Report IRK 76/01, IRK Vienna 1976

[23] M. Avrigeanu, V. Avrigeanu: Report NP-86-1995, IPNE Bucharest 1995

[24] H. Lenske *et al.*: *ibid.* [5], p. 110

[25] A. Marcinkowski, D. Kielan: *Nucl. Phys. A* **578** (1994) 168